2005 American Control Conference
June 8-10, 2005. Portland, OR, USA

Estimating relative deposition in a multi-zone process using a single composition sensor

Matthew J. Hilt, Tyrone L. Vincent, Bharat S. Joshi and Lin J. Simpson

Abstract— **When only a single composition sensor is available for a multi-zone co-evaporation process, it is difficult to determine the relative amount of material deposited in each zone. In this paper, a method of estimating the deposition-rate ratio between zones using small signal perturbation sequences is presented that exploits the exponential dependence of deposition rate on the temperature of the molten metal. A quality metric for the ratio estimate is presented, which can be easily calculated. Then, in order to determine the best perturbation sequence that meets all manufacturing constraints, a constrained optimization problem is described that is shown to be convex. An interesting feature of the solution is the importance of correlations between perturbation inputs. Experimental and simulation results are presented to validate the method.**

I. Introduction

An attractive option for low cost manufacturing of thin film components such as photovoltaic cells is semi-continuous, or roll to roll, processing using co-evaporation sources [1], [2]. In this setup, a flexible substrate is moved over multiple deposition zones, where in each zone effusion boats create a metal vapor plume by heating a sample to high temperature. The substrate is unrolled from one reel and taken up by another, and processing can continue until the reels need to be changed. The total thickness and relative composition of the deposited material can be measured before final take-up.

In multi-source co-evaporation systems the same metal may be deposited in more than one deposition zone, and different deposition rates may be desired. While the final thickness and composition is measured, this only gives the total amount of a particular material deposited over all zones. The relative amount of material deposited in a particular zone has the potential to be measured using alternative sensors such as atomic absorption spectroscopy or quartz crystal monitors [3], but conditions in the deposition chamber, cost, or complexity may prohibit their use in commercial production units. The relative rates could also be measured by shuttering individual sources in sequence, but the product produced during the shuttering must be scrapped. The following question thus arises: Can the relative deposition rates be determined using only a single composition measurement, while at the same time producing acceptable material?

The main contribution of this paper is the presentation of a method of estimating ratios of deposition rates in evaporation processes that exploits the exponential dependence of effusion rate on the temperature of the molten metal. This exponential dependence allows one to relate deposition rate to the sensitivity of deposition rate to changes in temperature. By modifying the temperature control of the effusion boats, the required sensitivity information can be extracted by perturbing the effusion cell temperatures, and then correlating the output deviations to the temperature disturbances. On the other hand, perturbations are undesirable in a manufacturing environment, and the perturbations will have to meet constraints imposed by the manufacturing tolerances. The optimal perturbation sequence will be one that maximizes the accuracy of the relative deposition rate estimate, while meeting all manufacturing constraints.

What we are left with is a problem of input optimization, which has been the subject of great attention in the system identification literature, see for example [4], [5] and the references therein. However, the ratio estimates that will be considered here contain unique complicating features. Thus, a secondary contribution of this paper is the presentation of an alternative performance metric for ratio estimates which can be easily calculated, and leads to a convex optimization problem. An interesting feature of the solution is the importance of enforcing correlations between perturbation inputs in different zones.

A. Notations

For a vector $x \in \mathbb{R}^n$, x^T indicates transpose, $\|x\| := \sqrt{x^T x}$, and $\|x\|_Q := \sqrt{x^T Q x}$. Given $x \in \mathbb{R}^2$, define $\text{ratio}(x) := \frac{x_1}{x_2}$, the ratio of the first element over the second. For a random vector x, let

$$\text{cov}(x) = E[(x - E[x])\,(x - E[x])^T] \tag{1}$$

indicate covariance, where E is expectation. For a vector sequence $u[k]$, $k = 1, \cdots, N$, let $\bar{E}(u[k]) = \frac{1}{N}\sum_{k=1}^{N} u[k]$ be the sample mean and

$$\overline{\text{cov}}(u^1[k], u^2[k]) = \frac{1}{N}\sum_{k=1}^{N}(u^1[k] - \bar{E}(u^1[k]))(u^2[k] - \bar{E}(u^2[k]))^T \tag{2}$$

This work was supported by National Science Foundation grant ECS-0134132 and Department of Energy Photovoltaic Manufacturing Technology Program DE-ZDO-2-30628-07.

M. Hilt and T. Vincent are with the Divison of Engineering, Colorado School of Mines, Golden, CO 80401, USA {tvincent|mhilt}@mines.edu

B. Joshi and L. Simpson are with ITN Energy Systems, Littleton, CO 80127, USA {bjoshi|lsimpson}@itnes.com

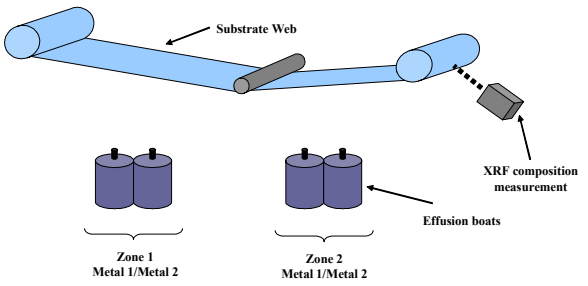

Fig. 1. Chamber diagram

(biased) sample covariance. Given a symmetric matrix $P \in \mathbb{R}^{n\times n}$, $P > 0$ indicates P is positive definite, i.e. $x^T P x > 0$ for all $x \neq 0$, and $P \geq 0$ indicates a positive semi-definite matrix. Given positive definite matrix P, let $P^{\frac{1}{2}}$ be the unique symmetric matrix such that $P^{\frac{1}{2}}P^{\frac{1}{2}} = P$ and let $P^{-\frac{1}{2}}$ be the inverse of this factor.

II. Web Deposition Process

A diagram of the interior of the deposition chamber is shown in Fig. 1. A flexible substrate is continuously transported through several different deposition zones, although only two are shown in the figure for simplicity. In-situ X-Ray Florescence [1] (XRF) is used to measure the composition of the deposited film as it leaves the last deposition zone. The XRF reports film thickness and composition every T_s seconds, and the result is an average of the material which has passed under the device during that time. A typical control strategy uses a fast PID control loop to power in order to keep a thermocouple measurement at a given set-point. The set-point is determined using the composition measurement.

In what follows, the following assumptions are utilized:

- The PID control loop is fast enough that temperature can be considered directly actuated.
- The transport distance between the individual zones and the XRF measurement point are known.
- The deposition rate is proportional to effusion rate.
- The composition measurement noise is zero-mean, white, and Gaussian.

When identifying variables in the model, the following convention will be used: The zone will be identified by a superscript, while the metal will be identified by a subscript. For example, the perturbation sequences used in zone i for metal m will be identified by u_m^j.

A. Deposition Rate Model

The effusion cells used in the deposition system are large ceramic boats filled with metal and heated using resistance heaters. Assuming molecular flow, the metal flux in molecules per second per meter squared is given by the Knudsen equation [6] $Q = \frac{N_A}{\sqrt{2\pi m R\tau}} p$ where N_A is Avogadro's number, m is the molecular weight in kg, R is the gas constant, τ is the temperature in degrees K and p is the pressure in N/m^2. Assuming supersaturation conditions within the boat, p will be given by the vapor pressure, which for many metals has the form $p = \frac{1}{\tau^c}\exp\left(a - \frac{b}{\tau}\right)$ for some constants a, b, c that depend on the metal. The effusion rate, r_e, in molecules per second, is then the product of the flux and the boat orifice area A, and the temperature will be the same as the temperature of the surface of the melt pool, τ_{melt}, so that

$$r_e = \frac{\kappa \exp(a)}{(\tau_{\text{melt}})^{c+0.5}} \exp\left(-\frac{b}{\tau_{\text{melt}}}\right) \tag{3}$$

where $\kappa = \frac{AN_A}{\sqrt{2\pi m R}}$. For typical operating conditions, the $(\tau_{\text{melt}})^{c+0.5}$ term is much less important than the exponential, and the effusion rate r_e can be approximated by a simple exponential. Thus, also using the stated assumption that deposition rate is proportional to effusion rate, in what follows we will use the expression $r = \delta\eta \exp\left(-\frac{b}{\tau_{\text{melt}}}\right)$ for deposition rate, where δ is a proportionality constant.

Assume that the melt temperature τ_{melt} is measured using a thermocouple with the measurement relationship $\alpha\tau + \beta = \tau_{\text{melt}}$, where τ is the thermocouple measurement, and α and β model measurement errors when $\alpha \neq 1$ or $\beta \neq 0$. The sensitivity of the deposition rate with respect to the measured temperature is then

$$\frac{dr}{d\tau} = \frac{\alpha b}{(\tau_{\text{melt}})^2}\delta\eta \exp\left(\frac{-b}{\alpha\tau + \beta}\right) = \frac{\alpha b}{(\tau_{\text{melt}})^2} r. \tag{4}$$

Note that the deposition rate is proportional to this sensitivity.

Now we consider multiple effusion boats, with the superscript/subscript notation distinguishing the metal and boat number for each variable. Consider two deposition rate sensitivities, $\frac{dr_m^i}{d\tau}$ and $\frac{dr_m^j}{d\tau}$, for the same metal m, but different boats i and j. If the same metal and type of effusion boat are used $b_m^i \approx b_m^j$, and if the thermocouple type and thermocouple placement allow for $\alpha_m^i \approx \alpha_m^j$,we have

$$\frac{\frac{dr_m^i}{d\tau}}{\frac{dr_m^j}{d\tau}} = \left(\frac{\tau_{\text{melt}}^j}{\tau_{\text{melt}}^i}\right)^2 \frac{r_m^i}{r_m^j} \tag{5}$$

so that the relative deposition rate $\frac{r_m^i}{r_m^j}$ is proportional to the ratio of sensitivities, with a correction factor equal to the ratio of melt temperatures squared. Usually, the melt temperatures are fairly close - due to the exponential, a wide range of deposition rates can be achieved with a small change in temperature. Typical correction factors will be of the range $0.8 - 1.2$, and can be estimated from the nominal operating conditions. *None of the parameters defining the vapor pressure, nor the error constants defining the thermocouple need to be known!*

B. Small Signal Deposition Model Structure

We consider obtaining estimates of the sensitivity via parametric system identification of the small signal dynamics between thermocouple temperature set-point and deposition rate. The metal is transmitted to the substrate in a

plume [6] whose shape will result in a particular deposition pattern. Let $y_m[k]$ be the deviation of the k^{th} sample of the XRF measurement of metal m from nominal. Let $u_m^i[k]$ be the k^{th} sample of the temperature deviation at zone i. Note, we assume that both input and output signals will have sampling time T_s, equal to the sampling time of the measurement. Also, we assume signals are synchronized so that the temperature deviation of sample k occurs $\frac{\ell^i}{v}$ seconds before the measurement of sample k, where v is the velocity of the substrate, and ℓ^i is the distance (along the substrate) from the effusion boat in zone i to the measurement.

Then, it can be shown that the small signal behavior due to deposition at n_z different zones be captured using moving-average models of the form.

$$y_m[k] = \phi_m^1[k]\theta_m^1 + \phi_m^2[k]\theta_m^2 + \cdots \phi_m^{n_z}[k]\theta_m^{n_z} \quad (6)$$

where

$$\phi_m^i[k] = \begin{bmatrix} u_m^i[k-n_1] & \cdots & u_m^i[k-n_2] \end{bmatrix} \quad (7)$$

n_1 and n_2 are constant integers, and ϕ_m^i are unknown parameters. The DC gain of this moving average model is equal to $\frac{dr_m^i}{d\tau}$.

III. Deposition Rate Sensitivity Ratio Estimate

In this section, we describe an estimate of the deposition rate sensitivity ratio based on system identification. Then, a measure for the width of the expected distribution for this estimate is defined. In the following sections, deposition sensitivity will be denoted as $s_m^i := \frac{dr_m^i}{d\tau}$, and the deposition sensitivity ratio defined as $g_m^{ij} := \frac{s_m^i}{s_m^j}$.

A. Sensitivity Ratio Estimate

For a particular experiment, perturbation sequences $u_m^j[k]$ are selected for each zone and each metal, and the composition perturbations $y_m[k]$ are measured. If data is recorded from $k = n_1$ to $N+n_2$, using (6), the input/output relationship for a particular metal can be written as

$$Y_m = U_m\Theta_m + E_m \quad (8)$$

where

$$Y_m = \begin{bmatrix} y_m[1] & y_m[2] & \cdots & y_m[N] \end{bmatrix}^T,$$

the other variables defined similarly, and E_m is the measurement error. When the perturbations are sufficiently small, the sensitivity s_m^j is equal to the sum of the elements of θ_m^j, that is, the DC gain of the small signal model. Thus $s_m^j = a_m^j\Theta_m$where a_m^j is a vector of ones and zeros that sums the appropriate elements of Θ_m, and from (5), $g_m^{ij} = \frac{s_m^i}{s_m^j} = \frac{a_m^i\Theta_m}{a_m^j\Theta_m}$.

Let $\hat{\Theta}_m = \left(U_m^TU_m\right)^{-1}U_m^TY_m$ be the least squares estimate of Θ_m. When the noise process is zero mean and white and $\lambda I = \mathrm{cov}(e)$, the covariance of this estimate is given by

$$\mathrm{cov}\left(\hat{\Theta}_m\right) = \lambda\left(U_m^TU_m\right)^{-1}. \quad (9)$$

With $\hat{s}_m^i = a_m^i\hat{\Theta}_m$ and $\hat{s}_m^j = a_m^j\hat{\Theta}_m$, our sensitivity ratio estimate is defined to be $\hat{g}_m^{ij} = \frac{\hat{s}_m^i}{\hat{s}_m^i}$. From the sensitivity ratio estimate, the deposition ratio estimate is given by $\left(\frac{\tau_{\text{melt}}^i}{\tau_{\text{melt}}^j}\right)^2\hat{g}_m^{ij}$, where τ_{melt}^i and τ_{melt}^j are considered known.

In the next section, the expected distribution of $\hat{g}_m^{ij}$ is found.

B. Distribution of ratio estimate

Let the joint probability distribution of the sensitivity estimates $\hat{s}^i, \hat{s}^j$ be $p_s(\hat{s}^i, \hat{s}^j)$. If $\hat{g} = \frac{\hat{s}^i}{\hat{s}^j}$, then the probability density function of $\hat{g}$ will follow the ratio distribution, given by

$$p_g(g) = \int_{-\infty}^{\infty} |\hat{s}^j| p_s(g\hat{s}^j, \hat{s}^j)\ \mathrm{d}\hat{s}^j \quad (10)$$

A good choice of input excitation will result the distribution $p_g(g)$ being narrow in some sense. However, when $\hat{s}^i$ are Gaussian, because the tail of this distribution decreases slowly, second moments of this distribution do not exist, and the variance cannot be calculated. We propose an alternate characterization of distribution "width" based an ellipsoidal bound of the expected estimates.

Suppose that it is known that the estimates satisfy

$$(s - s_{nom})\,Q(s - s_{nom}) \le \delta^2 \quad (11)$$

for some δ and positive definite Q. A hard constraint can be derived using an a-priori bound on the measurement noise, or it can be given a stochastic interpretation, for example if the estimates are jointly Gaussian, with covariance P and mean s_{nom}, then with $Q = P^{-1}$, $\hat{s}$ satisfies this constraint with probability $1 - \exp\left(-\frac{\delta^2}{2}\right)$ [7, p. 77]. Let $\mathcal{E}$ denote the set of points satisfying (11). We assume that δ is chosen small enough so that all elements of $s \in \mathcal{E}$ are strictly positive (i.e. s is in the open first quadrant). Recall that $\mathrm{ratio}(s)$ is the ratio of the elements of s. Clearly, there are points $s_{\max}$ and $s_{\min}$ in $\mathcal{E}$ such that $\mathrm{ratio}(s_{\max}) \ge \mathrm{ratio}(s)$ and $\mathrm{ratio}(s_{\min}) \le \mathrm{ratio}(s)$ for all $s \in \mathcal{E}$. Let $\phi_{\max}(Q) = \mathrm{ratio}(s_{\max})$ and $\phi_{\min}(Q) = \mathrm{ratio}(s_{\min})$. The difference $\phi(Q) = \phi_{\max}(Q) - \phi_{\min}(Q)$ between these points is a convenient measure of the spread of the ratio estimate distribution.

As examples, the maximum and minimum points are illustrated in Fig. 2 for $\sigma_1 = .1, \sigma_2 = .15$ and $\rho = 0$ and in Fig. 3 for $\sigma_1 = .1, \sigma_2 = .15$ and $\rho = 0.5$. The top graph shows the ellipse $\mathcal{E}$ for $\delta = 2$ (probability of .86) along with $s_{\max}$ and $s_{\min}$. The dashed lines denote values of s which also share the same ratio as the maximum or minimum ratio in $\mathcal{E}$. The bottom graph shows the corresponding ratio distribution if the random variables were jointly Gaussian, along with the value of ϕ, and the locations of $\mathrm{ratio}(s_{\max})$ and $\mathrm{ratio}(s_{\min})$. Note how the bounds reasonably reflect the relative breadth of the ratio distributions. It is interesting to note that although σ_1 and σ_2 are the same in both figures, the distribution for Fig. 3 is narrower, where a correlation exists between the sensitivity estimates. *The correlation significantly improves the ratio estimate!*

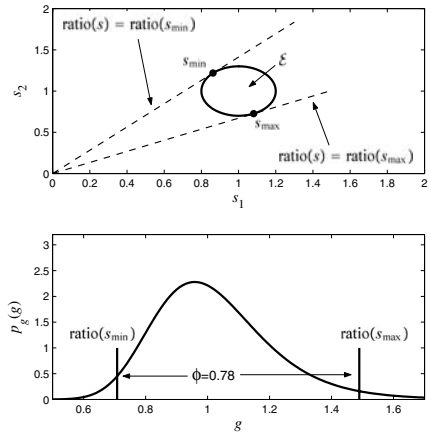

Fig. 2. Ratio distribtuion with uncorrelated sensitivity estimates

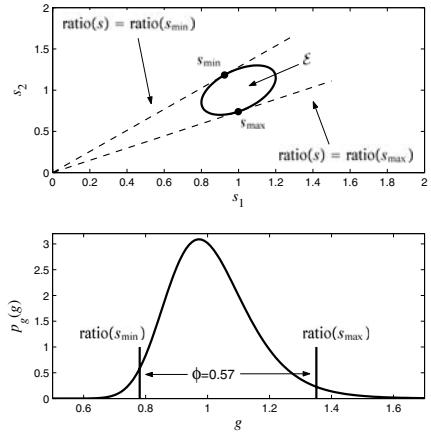

Fig. 3. Ratio distribution with correlated sensitivity estimates

Now, since Q is a function of the perturbation sequence used in the identification process, the quality measure ϕ can be influenced by appropriate choice of input. Significantly, ϕ has very nice properties that will be important in the optimization process: it has convex domain, it is easily computable, and it is convex over the space of symmetric matrices. Given s_{nom} and δ, let $\mathcal{D}$ be the set of Q such that $\mathcal{E}$ lies in the open first quadrant.

Theorem 1: For $s_1, s_2 \in \mathcal{E}$ defined by (11), if $Q \in \mathcal{D}$,

$$\phi_{\max}(Q) = \text{ratio}(\delta Q^{-1} w^{+} + s_{nom}) \quad (12)$$

$$\phi_{\min}(Q) = \text{ratio}(\delta Q^{-1} w^{-} + s_{nom}) \quad (13)$$

where

$$w^{\pm} = -Q^{\frac{1}{2}} \begin{bmatrix} \delta & \mp\sqrt{\gamma^2 - \delta^2} \\ \pm\sqrt{\gamma^2 - \delta^2} & \delta \end{bmatrix} \frac{Q^{\frac{1}{2}} s_{nom}}{\gamma^2} \quad (14)$$

and $\gamma = \left\| Q^{\frac{1}{2}} s_{nom} \right\|$. Furthermore, $\mathcal{D}$ is a convex set and $\phi(Q)$ is a convex function of Q

Proof: Due to space limitations, the proof is omitted. ■

IV. Process Constraints

In general, the performance metric $\phi(Q)$ can be made smaller by picking perturbation sequences with larger magnitudes. However, process tolerances will place constraints on how large the perturbations can be. The following constraints will be considered: the variance of a particular metal deposited in a particular zone, and the variance of key combinations of metals across zones.

Multi-source evaporation is used to create a graded film deposition, thus the total amount deposited in each zone is clearly important. However, other factors can also can also play an important role [8]. As examples, in deposition of high efficiency $CuIn_{1-x}Ga_xSe_2$ PV films, the choice of Cu to In+Ga ratio at a particular film depth is important, thus in a particular zone, it would be desired to minimize the variance of the sum In+Ga. On the other hand, the overall Cu to In ratio throughout the film is important, thus variation in total amount of a particular metal deposited in all zones should be minimized.

V. Optimal Input Sequence Selection

Using the measure $\phi(Q)$ and the process constraints described above, a perturbation sequence can be selected so that $\phi(Q)$ is minimized while the constraints are met. Let n_m be the number of different metals deposited in the chamber, n_z be the number of different zones, $n_s = n_m n_z$, and $n_\ell = n_2 - n_1$ be the number of terms in the small signal models of the deposition.

The problem is simplified by assuming that the input sequences have the characteristics of a zero mean and white random sequence through a shift of n_ℓ. That is, $\bar{E}\left(u_m^j[k]\right) = 0$ and In practice, these requirements will only be met approximately. A vector input sequence that can (approximately) achieve these requirements is easily generated using a maximum length pseudo random binary sequence (PRBS). For N large, these sequences are approximately white and zero mean. See for example [9] for algorithms to generate a PRBS and proofs of the stated properties. Define

$$S = \begin{bmatrix} s_{11}^{11} & \cdots & s_{n_m n_m}^{1 n_z} \\ \vdots & \ddots & \vdots \\ s_{n_m n_m}^{n_z 1} & \cdots & s_{n_m n_m}^{n_z n_z} \end{bmatrix} \quad (15)$$

It is assumed that $S \geq 0$.

Now, the performance metric and constraints can be expressed in terms of S or the elements of S. In particular, $Q = P^{-1} = \frac{N}{\lambda n_\ell}\left[A_m^{ij} S \left(A_m^{ij}\right)^T\right]$ where A_m^{ij} picks out the elements of S associated with metal m and zones i and j. Also, the constraints discussed in Section IV can be expressed as $\overline{\text{cov}}\left(y_m^i\right) = \left\|\theta_m^i\right\| s_{mm}^{ii}$ or

$$\overline{\text{cov}}\left(y_{mn}^{ij}\right) = \left\|\theta_m^i\right\|^2 s_{mm}^{ii} + \left\|\theta_n^j\right\|^2 s_{nn}^{jj} + 2\left(\theta_m^i\right)^T \theta_n^j s_{mn}^{ij} \quad (16)$$

where y_{mn}^{ij} is the sum of deposition by two specific effusion cells. Note that the elements of S appear linearly in

the process constraint expressions. Thus, n_c manufacturing constraints can be expressed as $f(S) \leq c_0$ for some linear function $f : \mathbb{R}^{n_s \times n_s} \to \mathbb{R}^{n_c}$ and $c_0 \in \mathbb{R}^{n_c}$ a vector of constraint bounds. Examining the bound (16) closely shows that correlation between input sequences will play an important role in meeting constraints. By the nature of the deposition process, θ_m^i and θ_n^j will have positive elements, and typically will be approximately equal. Therefore, if s_{mn}^{ij} is negative, the sample variance of key combination y_{mn}^{ij} will be reduced.

Given λ, δ, s_{nom}, N, and the nominal θ, characteristics of the the input sequence that minimizes the width of the ratio estimate distribution while meeting the manufacturing constraints can be found via the following constrained optimization problem over symmetric matrices S of appropriate dimension:

$$\begin{array}{ll} \min_S & \phi\left(\frac{N}{\lambda n_\ell}\left[A_m^{ij} S \left(A_m^{ij}\right)^T\right]\right) \\ \text{subject to} & f(S) \leq c \\ & S \geq 0 \end{array} \tag{17}$$

Since the objective function is a composition of a linear function (of S) and a convex function, it is convex. Since the constraints are also convex, this is a convex optimization problem. Once a solution to this optimization problem has been obtained, the desired sample covariance of the perturbation sequence is available in the minimizing S.

VI. Experimental and Simulation Results

In this section, we will attempt to partially validate the stated assumptions, and illustrate some of the advantages of a designed perturbation experiment. In order to examine the validity of (5), experimental data from an industrial deposition system is presented. However, when examining estimate distributions, simulations will be used because the large number of runs that are required.

A. Experimental Results

A perturbation experiment was performed by Global Solar Energy (GSE) in Tucson, Arizona on a co-evaporation system used to deposit $CuIn_{1-x}Ga_xSe_2$ films for production of high-efficiency flexible photovoltaic panels. The experiment perturbed the temperature set-point for a metal that is deposited in two different zones. Data was collected for 67 samples, so that with a sampling time of the composition sensor of $T_s = 120$ seconds, the experiment lasted a little over 2 hours. The perturbation sequences and resulting composition variation is shown in Fig. 4. Note, the input and output have not been aligned, so there is a delay of between 450 to 850 seconds from the input to the output due to substrate transport.

Small signal models were identified with $n_\ell = 3$. The input and output data was pre-filtered with a high pass filter to remove slow drifts in the composition not related to the inputs. The estimated sensitivity ratio was 2.16. The correction factor calculated from nominal operating temperatures was 1.12, so the estimated deposition ratio was 2.42. Although the relative thicknesses deposited in the two zones for standard depositions is proprietary to GSE, for the experimental run of this study the ratio of 3.51 was measured using shuttering. Although the estimates differ by 31% the change small signal sensitivity at the different deposition rates is apparent. Error analysis indicates that the difference in estimates can be explained by measurement noise.

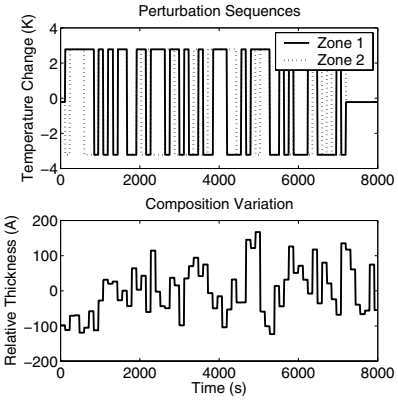

Fig. 4. Perturbation experiment and resulting composition variation

Variance bound	Zone 1	Zone 2	Total
Indium	100^2 Å^2	100^2 Å^2	50^2 Å^2
Gallium	100^2 Å^2	20^2 Å^2	50^2 Å^2
In + Ga	50^2 Å^2	50^2 Å^2	None Specified

TABLE I
Acceptable thickness variations for each metal in each deposition zone

B. Simulation Results

The simulated system consists of two metals and two zones. Indium is metal 1 and Gallium is metal 2. For simplicity, the outer-loop temperature set-point control is eliminated and melt temperature is considered directly actuated. Effusion model is (3), with parameters given in Table II. For these parameters, the nominal relative metal deposition ratio is 1.8. The plume model for all metals and zones is

$$f(x) = \frac{1}{\sqrt{2\pi}\frac{v}{30}} \exp\left(-\frac{1}{2}\frac{x^2}{\left(\frac{v}{30}\right)^2}\right) \tag{18}$$

Parameters	Indium	Gallium
κ	1.71×10^6	3.00×10^6
a [10]	9.79	10.07
b [10]	12580	14700
$\bar{\tau}^1$,$\bar{\tau}^2$ °K	1280,1200	1350,1225

TABLE II
Parameters for simulation

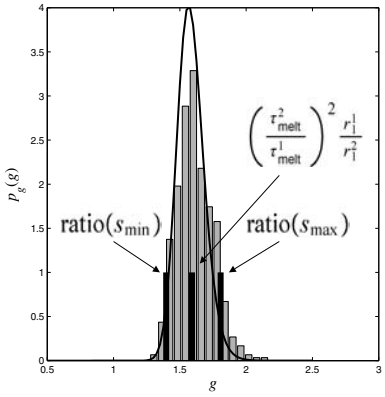

Fig. 5. Scaled histogram of sensitivity ratio estimates, along with expected distribution, predicted ratio bounds, and actual ratio.

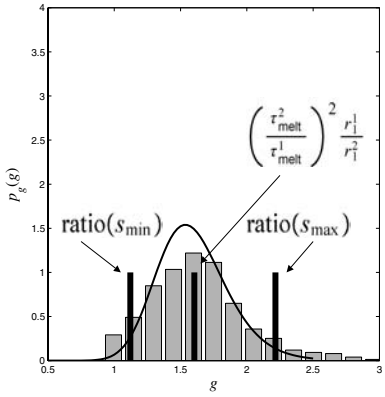

Fig. 6. Results for input with sample covariance S_c

Noise is chosen to be $\lambda = 30^2$, and $N = 63$. The model parameters are $\theta^i_m = \frac{dr^i_m}{d\tau}\begin{bmatrix}0.1 & .8 & 0.1\end{bmatrix}$ .and we calculate

$$\frac{dr^1_1}{d\tau} = 12.73 \quad \frac{dr^2_1}{d\tau} = 8.05 \tag{19}$$

$$\frac{dr^1_2}{d\tau} = 7.18 \quad \frac{dr^2_2}{d\tau} = 3.19 \tag{20}$$

In practice, these would be found from an initial system identification experiment. We seek an experiment which can estimate the ratio of Indium deposition rate in zone 1 to zone 2. Processing constraints are in Table I, which reflect constraints on the variance in both the total deposited metal, as well as various combinations between zones and between metals. Optimization results in

$$S = \begin{bmatrix} 66.2 & -70.0 & -50.3 & 49.9 \\ -70.0 & 114.5 & 37.6 & -82.6 \\ -50.3 & 37.6 & 44.2 & -26.4 \\ 49.9 & -82.6 & -26.4 & 59.6 \end{bmatrix} \tag{21}$$

and inputs are generated using PRBS sequences to approximately satisfy this sample covariance. Note the significant correlation between inputs. After simulation, 500 different realizations of simulated white Gaussian noise was added to the composition measurement, and then for each realization, sensitivity estimates were obtained. In Fig. 5, we show a histogram of the resulting sensitivity ratio estimate, along with the theoretical ratio distribution, and the actual deposition rate ratio scaled by $\left(\frac{\tau^2_1}{\tau^1_1}\right)^2$. Note that the agreement between the actual and theoretical results is very good.

For comparison, consider a sample covariance matrices chosen as follows:

$$S_c = \text{diag}\left(\begin{bmatrix}13 & 33.5 & 0 & 0\end{bmatrix}\right) \tag{22}$$

The second input was chosen without correlation, and scaled so that all constraints are met (within the same tolerance as the optimal input) - is this essentially the best possible input if no correlation is allowed. The results for the optimal and comparison inputs are listed in Table III. The distribution for the second input is shown in Fig. 6, and as expected, the distribution is significantly wider than the optimal input.

Achieved Variances	"Optimal" Input	Comparison Input
Indium Zone 1	83.8^2 Å^2	36.2^2 Å^2
Indium Zone 2	70.3^2 Å^2	36.4^2 Å^2
Indium Total	50.8^2 Å^2	50.8^2 Å^2
Gallium Zone 1	39.0^2 Å^2	0 Å^2
Gallium Zone 2	20.1^2 Å^2	0 Å^2
Gallium Total	33.9^2 Å^2	0 Å^2
In + Ga Zone 1	49.9^2 Å^2	36.2^2 Å^2
In + Ga Zone 2	50.3^2 Å^2	36.4^2 Å^2

TABLE III
RESULTS FOR THICKNESS VARIATIONS FOR SELECTED INPUTS

VII. ACKNOWLEDGMENTS

The authors thank Jane VanAlsburg-Westermann, Scott Wiedeman and Jeff Britt of Global Solar Energy for their assistance in obtaining the experimental results.

REFERENCES

[1] I. Eisgruber, B. Joshi, N. Gomez, J. Britt, and T. Vincent, "In-situ x-ray fluorescence used for real-time control of $CuIn_xGa_{1-x}Se_2$ thin film composition," *Thin Solid Flims*, vol. 408, pp. 64–72, 2002.

[2] S. T. Junker, R. W. Birkmire, and F. J. Doyle, III, "Manufacture of thin-film solar cells: Modeling and control of $Cu(InGa)Se_2$ physical vapor deposition onto a moving substrate," *Ind. Eng. Chem. Res.*, vol. 43, pp. 566–576, 2004.

[3] B. Utz, S. Rieder-Zecha, and H. Kinder, "Continous $YBa_2Cu_3O_{7-\delta}$ film deposition by optically controlled reactive thermal co-evaporation," *IEEE Trans. Applied Superconductivity*, vol. 7, no. 2, pp. 1181–1184, 1997.

[4] R. K. Mehra, "Optimal input signals for parameter estimation in dynamic systems - a survey and new results," *IEEE Trans. Automatic Control*, vol. AC-19, pp. 753–768, 1974.

[5] G. C. Goodwin and R. L. Payne, *Dynamic System Identification: Exeriment Design and Data Analyisis*. New York: Academic Press, 1977.

[6] D. L. Smith, *Thin-Film Deposition: Principles and Practice*. New York: McGraw-Hill, 1995.

[7] H. L. Van Trees, *Detection, Estimation, and Modulation Theory*. New York: Wiley, 1968.

[8] R. W. Birkmire and E. Eser, "Polycristalline thin film solar cells: Present status and future potential," *Annu. Rev. Mater. Sci.*, vol. 27, pp. 625–53, 1997.

[9] T. Söderström and P. Stoica, *System Identification*. New York: Prentice Hall, 1989.

[10] E. A. Brandes and G. B. Brook, Eds., *Smithells Metals Reference Book*, 7th ed. Oxford: Butterworth Heineman, 1998.